Hindawi
Mathematical Problems in Engineering
Volume 2019, Article ID 7317520, 13 pages
https://doi.org/10.1155/2019/7317520

Research Article

Prediction of Slipper Pressure Distribution and Leakage Behaviour in Axial Piston Pumps Using ANN and MGGP

Özkan Özmen,[1] **Cem Sınanoğlu**,[1] **Turgay Batbat**,[2] **and Ayşegül Güven**[2]

[1]*Department of Industrial Design Engineering, Erciyes University, Kayseri 38030, Turkey*
[2]*Department of Biomedical Engineering, Erciyes University, Kayseri 38030, Turkey*

Correspondence should be addressed to Özkan Özmen; ozmen@erciyes.edu.tr

Received 24 December 2018; Accepted 12 February 2019; Published 4 March 2019

Academic Editor: Leandro F. F. Miguel

The pressure distribution (PD) and leakage between the slipper and swash plate in an axial piston pump (APP) have a considerable impact on the pump efficiency, affecting aspects such as the load bearing and wear performance of the slipper. Herein, multigene genetic programming (MGGP) and artificial neural network (ANN) machine learning methods (MLMs) are incorporated into a novel approach towards predictive modelling of the PD and leakage on the slipper, which can function hydrostatically/hydrodynamically. Experimentally measured data are used as input for the MGGP and ANN models. The validity of the MGGP and ANN models is verified using test data excluded from the analyses. In addition, the model results are compared with analytic equations (AEs). Both MLMs are found to exhibit strong agreement with the measured data. In particular, the ANN model exhibits superior prediction performance to the MGGP model and AEs.

1. Introduction

Axial piston pumps (APPs) are in frequent use because of their ability to operate under high-pressure conditions. Most of these devices require a swash plate and hydrostatic/hydrodynamic slipper to function. Therefore, the interaction between the slipper and swash plate affects the system performance directly.

Many studies on slipper behaviour modelling have been performed in the past 40 years, in which theoretical, analytical, numerical, and machine learning methods (MLMs) have been employed with the aim of improving APP performance. Considering the tilt, grooves, and rotational speed of the slipper and swash plate, Bergada et al. [1] developed new equations based on the Reynolds lubrication equation. In their model, the flow was considered to be dominant in the radial course and the fluid was taken to be incompressible. In addition, generalised equations for slippers with any number of lands were established. The analytic equations have proven to agree well with experiment data. In one of their studies, Bergada et al. [2] examined the behaviour of a slipper working hydrostatically/hydrodynamically and produced an analytical formulation based on the Reynolds lubrication equation. In addition, they supported this analytical formulation through experiment and implemented a fluid dynamics model. Similarly, by acknowledging that the slipper is parallel to the swash plate, Kumar et al. [3] developed a model capable of calculating fluid film pressure and leakage. That model was established considering the tangent speed for different groove sizes, using the complete Navier Stokes equations. The mean fluid thickness and PD for invariable and dynamic operating conditions were experimentally quantified and compared. Furthermore, under the assumptions that the space between the slipper and swash plate is fixed and that the slipper is nontilted and straight, Johnson and Manring [4] developed an analytic model based on classical lubrication theory, which also considers tangential speed. They observed that an increase in slipper pocket depth reduces friction. Tang et al. [5, 6] developed a numerical model for a hydrostatic slipper considering heat transfer and thermal effects. The established model was used to study the effects of the structural parameters and material properties on the hydrostatic bearing capacity.

In an experimental study, Canbulut et al. [7] investigated the power loss in APPs and the effect of surface roughness on the slipper. They designed an experiment setup to

determine the slipper performance under different operational conditions. Those researchers also observed that reduced surface roughness causes lower power loss and that the power requirement is reduced with increased orifice diameter and pressure. By varying the geometric features of the slipper and its operational parameters, Canbulut [8] studied the minimum frictional power loss and minimum oil leakage, again by considering the slipper surface roughness. Hence, it was observed that the frictional power loss and oil leakage depend on the surface roughness, turning speed, hydrostatic bearing area size, supply pressure, and orifice diameter. Lin and Hu [9] considered the slipper rotational speed, loading pressure, and oil viscosity and suggested a tribodynamic model. To obtain a solution to this model, they employed the niche genetic algorithm (GA). To quantify the oil film thickness, they designed a test setup and observed that the theoretical results and quantified results were in good agreement. Chao et al. [10] developed a new Reynolds equation, which considers the slipper spin, by employing the equilibrium equation and continuity equation. Those researchers demonstrated that their proposed Reynolds equation has the same form as its version in the literature; however, the equations differ completely according to the velocity boundary conditions. Moreover, in another study [11], the same researchers designed a new experimental setup for slipper spin and discovered that the slipper turning speed is almost equal to that of the shaft. Considering the interaction between the elastohydrodynamic behaviour and viscosity temperature, Tang et al. [12] developed a new thermoelastohydrodynamic lubrication model for the behaviour between the APP and slipper. They demonstrated that the calculated temperature and film thickness are in good harmony and that the pressure exhibits a reasonable distribution compared to earlier studies.

Nonlinear systems are difficult to model because of their characteristics and the associated problems and because prediction of their parameters is difficult [13]. MLMs are frequently used to overcome such difficulties. In MLMs, the relationship between the input and output data can be predicted easily, with no need for acceptance. In the literature, the artificial neural network (ANN) is one of the most commonly used modelling systems for slippers. Canbulut et al. [14] considered the orifice sizes and slipper pocket and developed an ANN model to analyse the system rigidity in a bearing. The results obtained for test data submitted to the trained network exhibited close agreement with the experiment results. In another study, Canbulut et al. [15] investigated the effects of different surface areas and surface roughness values on slipper performance; hence, they formed an ANN model using their empirical results. The empirical results for the leakage quantity were completely consistent with the ANN model. In addition, those researchers observed that the leakage quantity depends on the surface roughness, orifice diameter, bearing area size, supply pressure, and rotation speed. In another study, Canbulut et al. [16] investigated the frictional power loss, both theoretically and experimentally. They determined the minimum frictional power loss for different study parameters and slipper geometries. Additionally they demonstrated that the ANN model can be used in real time. Canbulut et al. [17] also used ANNs for analysis of hydrostatic circular recessed slippers. They correctly modelled the static and dynamic features of the slipper using the developed ANN model. Further, Liu et al. [18] calculated the form of the oil film through analysis of the power balance, by applying the niche GA and treating the calculation as an optimisation problem. Hence, they observed that the rotational speed has a significant effect on the film form.

Although ANNs exhibit good modelling performance when applied to slippers, they do not mathematically produce a function, as the network generally develops a model based on input and output data. In this study, we modelled the complex behaviours between the slipper and swash plate of an APP using MGGP and ANN. The PD on the slipper and the leakage were incorporated into the MGGP and ANN models. Further, the accuracies of both the ANN and MGGP models were tested on empirical data not used for analysis and the performance compared with that of analytic equations (AEs) produced from the Reynolds equation.

The remainder of this article is structured as follows. In Section 2, the APP working principle is briefly summarised. In Section 3, the experiment setup is described. In Section 4, the MGGP and ANN, parametric value selection, and performance criteria used in this study are discussed. In Section 5, the findings are presented and discussed. Finally, in Section 6, the conclusion is presented and future work is considered.

2. Theory of the System

Figure 1(a) presents an illustration of a typical APP. Each piston makes contact with the slipper via a ball-joint connection; these ball joints allow the pistons to remain parallel to the swash plate at all times. When working via the drive shaft, the pump turns the cylindrical block. The swash plate is oblique, which enables the pistons to move back and forth. A steady oil flow is created by the piston motion, which, in turn, generates pressure in the hydraulic network. Variation of the swash plate angle changes the piston stroke; hence, variable displacement is achieved. During operation, the piston is under the load of the pressurised oil. This load is transferred to the slippers through the orifice. The slipper bears this load and slips over the swash plate during the pump operation. At this point, if there is insufficient lubrication, metal-metal friction develops; also, excess oil flow reduces the system efficiency. Figure 1(b) shows the slipper and swash plate. With rotation of the swash plate, the oil in the piston is transferred to the slipper through the orifice and leakage occurs. As a result, the force created by the pressure in the slipper pocket diminishes somewhat. However, this reduction is compensated for by the compressive force developing on the slipper land, and the total pressure forces remain in balance.

As the supply pressure increases or decreases, the pocket pressure also increases or decreases. Thus, the thickness of the oil film between the slipper and swash plate adjusts, and the generated compressive force remains in constant balance. As apparent from Figure 1(b), the load capacity,

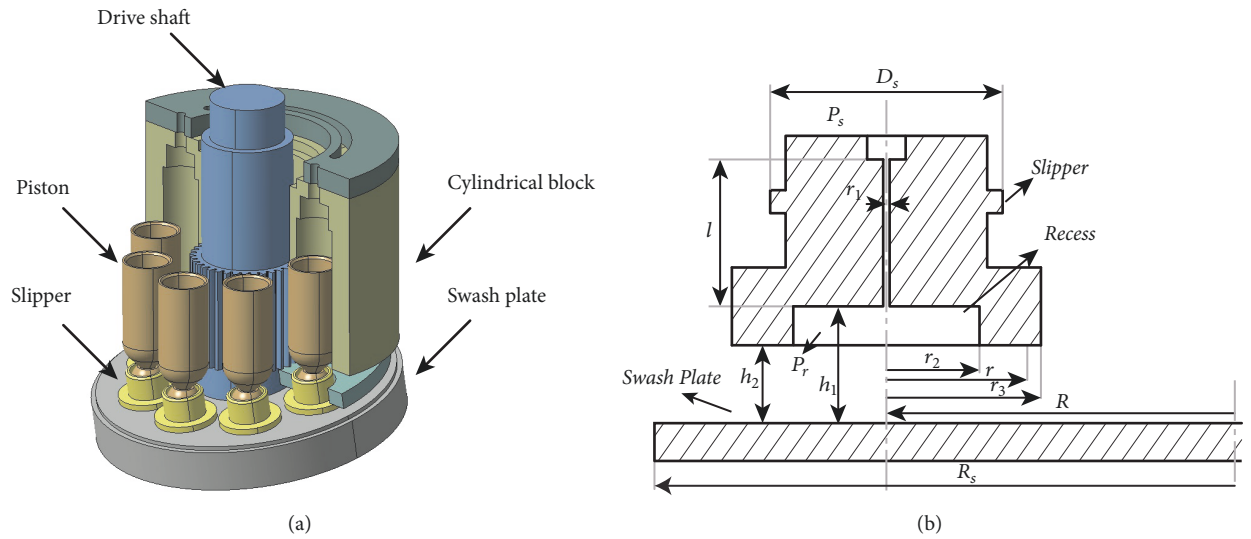

Figure 1: Schematic presentation: (a) axial piston pump and (b) slipper/swash plate used in this study.

which is caused by the supply pressure (P_s) and acts on the slipper, is balanced by the pressure between the slipper bearing surface and the anticoincident elements [7]. The PD on land under these circumstances can be explained through solution of the Reynolds equation in cylindrical coordinates for flat slipper including average oil film thickness [2]:

$$P = P_r - \frac{(P_r - P_{outlet})}{\sum_{i=1}^{i=2}(1/h_i^3)\ln(r_{i+1}/r_i)}\left[\frac{1}{h_1^3}\ln\left(\frac{r_2}{r_1}\right) + \frac{1}{h_2^3}\ln\left(\frac{r}{r_2}\right)\right] \quad (1)$$

where r_1 represents the radius of the orifice, r_2 the radius of the slipper pocket, r_3 the outer slipper radius, P_r the slipper pocket pressure, and P the pressure at any point on the slipper land. With the omission of the paralleling conditions between slipper/swash plate and η, the dynamic viscosity of the fluid, Q, is as follows:

$$Q = \frac{\pi}{6\eta}\frac{(P_r - P_{outlet})}{\sum_{i=1}^{i=2}(1/h_i^3)\ln(r_{i+1}/r_i)} \quad (2)$$

3. Experimental System

3.1. Experimental Setup. The experimental setup shown in Figure 2(a) was prepared based on the experimental setups in [14–17]. The apparatus consisted of a main test unit, a section in which measurements were performed and data acquired, and units supplying the system with pressurised oil.

3.1.1. Main Test Unit. The structure of the main test unit is shown in Figure 2(b). This unit comprised a hydraulic loading block, slippers, a swash plate, lowering shaft, micrometres, and oil inlet and outlet sections. Pressurised oil was forced into the system through the inlet. The oil discharged from the slippers was transported back to the oil tank.

3.1.2. Measurement of Data. The swash plate was prepared using steel that was quenched before its surface was ground. An axial ball-bearing was used for the swash plate, which was directly connected to a 5-kW servo motor (Mitsubishi MR-J2S-500A) for driving. The swash plate had a mean surface roughness of 1.33 μm and operated with a runout of 3–10 μm depending on the pressure and speed. As apparent from Figure 2(b), there were three slippers at an angle of 120°. Thus, each slipper was loaded equally. The slippers were made of brass and their dimensions are given in Table 1. The pressure measurement was performed for one of the slippers, while the slipper runout was measured for another slipper. There were four holes on the slipper created for pressure measurement (Figure 3).

One of these holes was located in the slipper pocket (labelled '4'), and the remaining three were positioned at 1.5 mm interior to the outer diameter and at an angle of 120° (Figures 3(a) and 3(b), labelled '1', '2', and '3'). For pressure measurement, 0.6-mm holes were opened on the slipper edges and copper pipes were welded to those holes. A Keller PA-21-SR 0-60-bar piezoresistive pressure sensor was used for measurement. In addition, another pressure sensor measured the supply pressure before oil entered the system. Figure 3(a) shows that a thermocouple was connected to the slipper (labelled '6'), while the temperature of the oil in the slipper was measured through the hole labelled '5'. Runout quantification was performed using a Mitutoyo Absolute Digimatic Indicator with an Output Comparator, which has a sensitivity of 1 μm. For the runout, mean values were used, because the rotation speed of the swash plate under the slipper is very high. All slippers were produced using the same manufacturing parameters, and an orifice of

Table 1: Slippers used in experiment.

Symbol	Parameter	Value
r_1	Radius of the capillary tube	0.45
r_2	Inner radius	12
r_3	Outer radius	20
r	Radius of pressure point	18.5
R	Rotation radius	45
R_s	Swash plate radius	86
r_{p_1}	Pressure point 1 of slipper from swashplate centre	48.5
r_{p_2}	Pressure point 2 of slipper from swashplate centre	30.8
r_{p_3}	Pressure point 3 of slipper from swashplate centre	61.3
D_s	Piston diameter	30
l	Length of the capillary tube	20
θ_1	Angle of the pressure point 1 from slipper center	4.71
θ_2	Angle of the pressure point 2 from slipper center	0.52
θ_3	Angle of the pressure point 3 from slipper center	2.62
b	Slipper/swash plate distance before experiment	3

∗unit of the lengths are mm.
∗∗unit of the angles are radian.

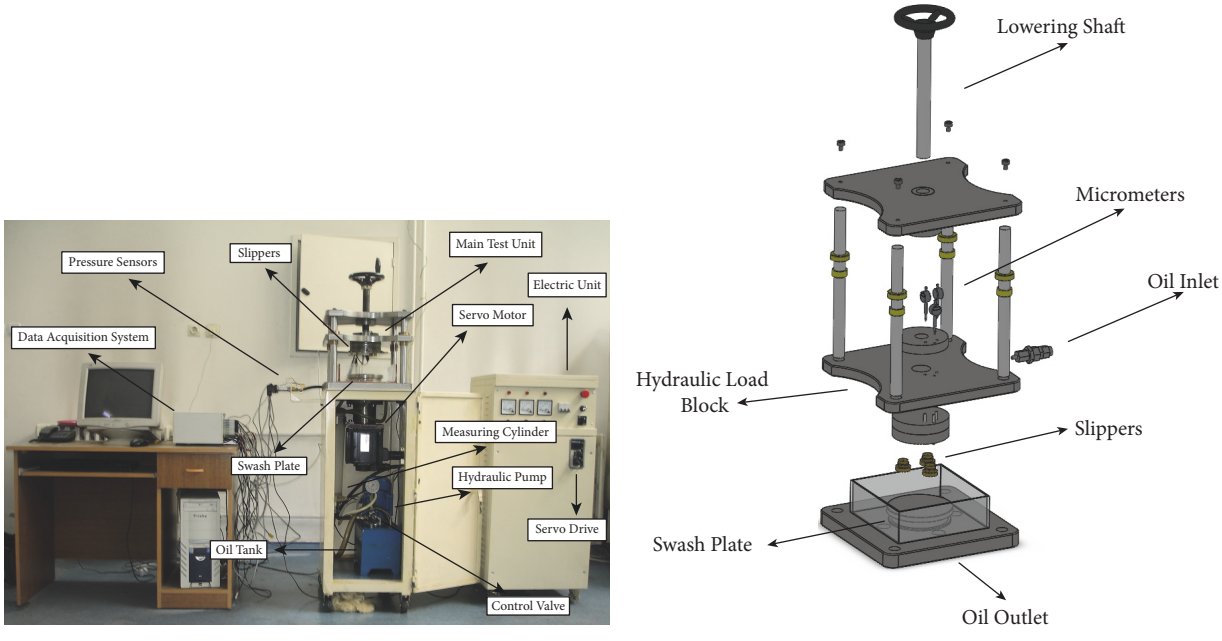

Figure 2: Experimental setup: (a) experiment set and (b) the disassembly appearance of experimental set.

0.9 mm in diameter was in the exact centre of the slipper (label '9'). Also, labels 7 and 8 in Figure 3(a) show slipper land and pocket, respectively. For data acquisition from the experiment setup, a 20-channel AHLBORN data logger was used (Figure 2(a)). The obtained data were processed in the electronic environment with the aid of the AMR WinControl program and adjustments were made such that one datum per second was recorded. In addition, two thermocouples were connected to the data logger: one to measure the oil temperature in the tank, and the other to measure the ambient temperature.

3.1.3. System Pressured Oil. A 0.37-kW Gamak AGM 71 4b motor with three phases was used to transport the pressurised oil to the experiment apparatus. Before sending oil to the apparatus, which incorporated a 25-L oil tank, the pressure was adjusted using a Bourdon gauge. The same pressure values were also read by means of a pressure sensor.

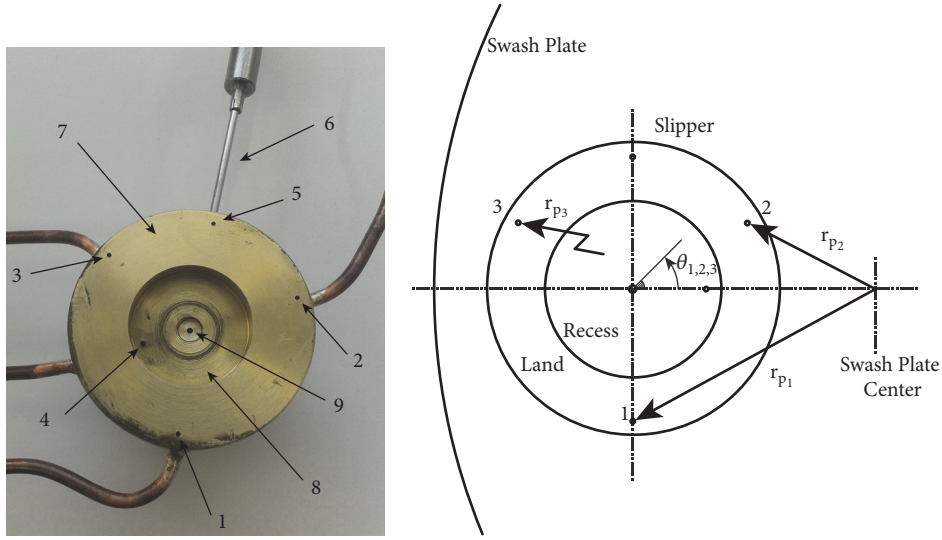

(a) (b)

Figure 3: Slipper: pressure measurement points (1-4), thermocouple and its hole (5-6), slipper land and pocket (7-8), and orifice (9).

3.2. Experimental Method. Before beginning the experiments, the hydraulic load unit was lowered via the lowering shaft until the space between the slipper and swash plate was 3 mm. Then, the pump in the apparatus was operated to transport the pressurised oil to the hydraulic load unit. First of all, the slipper goes down 3 mm and in this way the hydraulic load unit (lowest point) is guaranteed not to come into contact with the slipper (upper point of land) during operation. Thus, the slipper, moving freely up and down, balanced itself according to the required oil thickness. This oil generated pressure in the slipper pocket and slipper land. For PD modelling, supply pressures of 20, 30, 40, 50, and 60 bar were considered. Note that data could not be obtained at 10-bar pressure owing to insufficient oil flow at the measurement points. For leakage modelling, however, the 10–60-bar pressure range was considered. In addition, owing to the orifice diameter–slipper pocket–piston diameter ratio, the supply pressure in the system did not exceed 65 bars. As pressure measurement could not be performed at the pressure measurement points at high speeds, swash plate rotation rates of 0, 200, 400, 600, 800, and 1000 rpm were selected. During the experiment, the oil temperature was fixed at 25°C by means of an air-cooled system. Shell Tellus 68 hydraulic oil (η = 0,12278 Ns/m^2) was used as the fluid. Each experiment was repeated three times.

4. Material and Methods

4.1. ANN Model Development. ANNs inspired by the biological nervous system consist of process elements (artificial nerve cells) connected to each other. In an ANN, each connection has a certain weight, and the information possessed by the network is concealed in the weight values distributed throughout the network. An ANN generally has an input layer, one or more hidden layers, and an output layer (Figure 4). Data are brought to the network through the input layer, processed in the hidden layers, and sent to the output layer. The weight values of the network are determined through data processing and are also defined as part of the network learning [19].

4.1.1. Settings of Parameters of Proposed ANN Model. In this work, the ANN inputs were the data obtained from the experiment. The activation functions employed in this study are logarithmic sigmoid, hyperbolic tangent sigmoid, and pure linear activation functions (Eqs. (3)-(5)) most frequently used for similar problems in the literature [14–17].

$$logsig\,(x) = \frac{1}{(1 + e^{-x})} \tag{3}$$

$$tansig\,(x) = \frac{2}{(1 + e^{-2x})} - 1 \tag{4}$$

$$pureline\,(x) = x \tag{5}$$

In this study, two hidden layers were used to form the ANN model. For each activation function combination, the minimum error rate was determined based on the mean squared error (MSE) for 400 trials in

$$MSE = \sum_{i=1}^{N} \frac{(o_i - t_i)^2}{N} \tag{6}$$

where o_i represents the outputs of the ANN model, t_i the experimentally measured values, and N the number of test data elements. Figure 5 shows the errors obtained for 70% training data, 15% validation data, and 15% test data, when logarithm sigmoid, pureline linear, and tangent sigmoid activation functions were implemented in the input, hidden, and output layers, respectively. The trial and error PD results

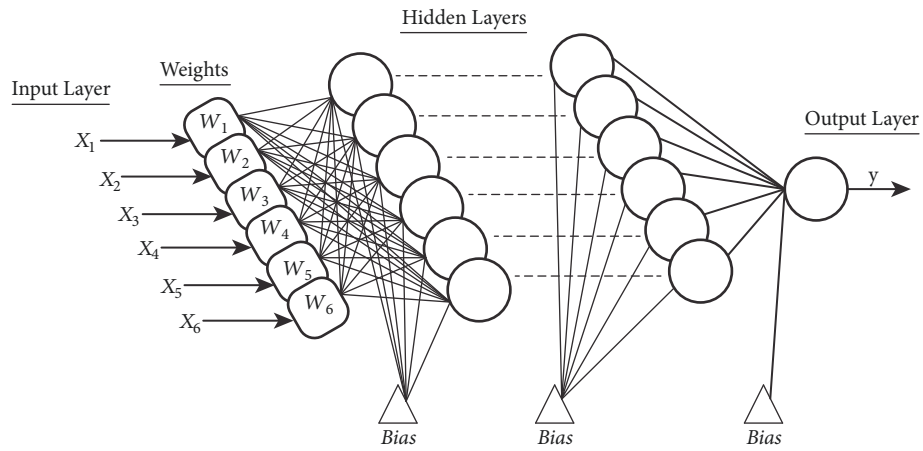

Figure 4: The framework of the proposed ANN.

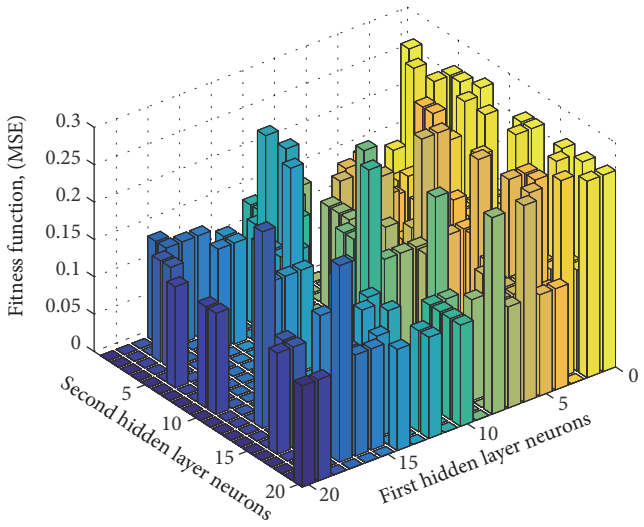

Figure 5: Error for number of neuron combinations in hidden tabs for an ANN model.

Table 2: Parameters of proposed ANN.

Parameters	Values
Training data set	4799
Validation data set	1028
Testing data set	1028
Number of hidden layers	2
Number of neurons in hidden layers	1-20
Activation functions	Tagsig-Logsig-Pureline
Number of epochs	10000
Learning rate	0.7
Architecture selection	Trial-Error
Target goal mean square error	10-7
Minimum performance gradient	10-7

of the ANN model are also shown. For this combination of activation functions, the network structure with the most favourable performance had 3.2153e-05 MSE; this result was achieved for a model with 13 and 7 neurons in the first and second layers, respectively.

The other models in the study were also similarly optimised using the trial and error method. Code developed in MATLAB was used. The ANN training and structural parameters are presented in Table 2. All three activation functions for the hidden and output layers were attempted in all combinations. Results were obtained for hidden layers with all neuron numbers between 1 and 20.

4.2. MGGP Model Development. First developed by Koza on the basis of the GA, GP is an MLM [20]. In GP, data are stored as computer programs in the form of tree structures containing functions and terminals. The functions may include mathematical functions (sin, cos, x, e^x, In, log, power, etc.), logic functions (AND, OR, NOT, NOR, XOR, etc.), arithmetic functions (+, -, x, and /), and programming functions. Terminals can contain input variables, quantitative variables, logical constants, etc. [21]. The function and terminal selection randomly generate an initial population. Then, a new population is produced according to a suitability function determined by means operators such as regeneration, mutation, and crossover. Thus, a tree structure with a minimised error ratio is obtained. This process continues until one of the defined stopping criteria is satisfied [22–26]. MGGP exploits a weighted linear combination of the outputs of a series of GP trees, for which each tree may be regarded as a gene. In the equation given in Figure 6, a, b, and c are input values; y is the output value; A_0 is the bias (offset) term; and A_1, A_2, and A_3 are gene weights.

4.2.1. Settings of Parameters of MGGP. Parameter adjustments have an important influence on the efficiency of

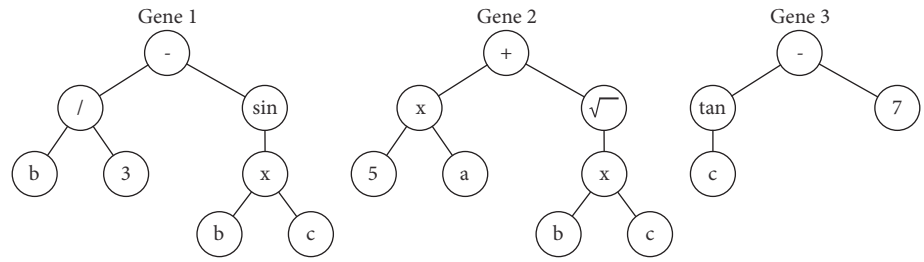

Figure 6: Example of a multigene genetic symbolic model.

Table 3: Parameters of proposed MGGP.

Parameters	Values assigned
Population size	100-500
Number of generations	100-400
Tournament size	15-20-25
Probability of Pareto tournament	0.5-0.6-0.7
Elite fraction	0.08-0.09-0.1
Maximum depth of tree	4-5-6
Max genes	4-5-6
Functional set (F)	+, −, ×, ÷, $\sqrt{}$, tanh, exp, log, abs, cube, negexp, mult, add, sqrt, neg
Terminal set (T)	(x1, x2, x3, x4, x5, x6 [−10 10])
ERC probability	0.1
Crossover probability rate	0.84
High-Level crossover	0.2
Low-Level crossover	0.8
Mutation probabilities	0.14

the MGGP algorithm. In this study, these parameters were identified with reference to the literature and are listed in Table 3. All combinations were implemented and a compact model with minimum error was sought.

The elements in the terminal set, the input values from the empirical data, and the random constants are selected randomly, taking experiment/human error with a range of [−10 10] into consideration [23]. It has been reported that restriction of G_{max} (the maximum gene number) and D_{max} (maximum tree depth) in particular enables evolution of relatively compact individuals, even if there are many inputs [27, 28]. Thus, in this study, G_{max} and D_{max} were set to six. In addition, it has been noted that the population number and generation number of the training data influence the MGGP performance for large datasets in different engineering applications [29–31]. Therefore, in the present study, the population size was in the 100–500 range, and generation numbers of 100 to 400 were studied, with increments of 100 in each instance. In this study, for multigene symbolic regression, the open source GPTIPS software developed in MATLAB was used [27]. The fitness values for the measured and predicted outputs were obtained using the root mean square error (RMSE) in GPTIPS (Eq. (7)) and a trial and error method similar to ANN.

4.3. Comparison of Performances of ANN and MGGP Models. The data obtained from the experiment described in Section 3 were used incorporated in the AEs, MGGP, and ANN. Before implementation, the dataset was mixed randomly and divided into three separate datasets, to obtain 70% training, 15% validation, and 15% test data. To evaluate the model performance, the following accuracy indexes were used: RMSE, the coefficient of determination (R^2), relative error (RE), mean absolute percentage error (MAPE), and multiobjective error (MO), as expressed in (7)–(11), respectively.

$$RMSE = \sqrt{\frac{1}{N}\sum_{i=1}^{N}(o_i - t_i)^2} \tag{7}$$

$$R^2 = 1 - \frac{\sum_{i=1}^{N}(o_i - t_i)^2}{\sum_{i=1}^{N}(o_i - \overline{o}_i)^2} \tag{8}$$

$$RE\,(\%) = \frac{|o_i - t_i|}{t_i} \times 100 \tag{9}$$

$$MAPE = \frac{1}{N}\sum_{i=1}^{N}\left|\frac{o_i - t_i}{t_i}\right| \tag{10}$$

$$MO = \frac{MAPE + RMSE}{R^2} \tag{11}$$

In cases where there are sufficiently large input and output datasets, R^2 becomes important. In this study, a total of 6855 data obtained from the experiment were used for PD analysis, while 2484 data elements were used for leakage analysis. Note that the proximity of R^2 to 1 shows the degree of agreement between the observed results and model outputs. However, if the data in the model change equally, R^2 does not change. The RMSE and MAPE indexes show the relative error, but not the correlation. Therefore, the MO error function, which is a combination of functions, was also used [32].

5. Results and Discussions

5.1. Pressure Distribution on the Slipper. The APP working conditions are some of the most important factors affecting the PD on the slipper. Supply pressure (P_s) is exerted as a downward force on the slipper. Oil (Q) flows into the slipper pocket through the orifice. This, in turn, creates an upward, recess pressure (P_r) and an opposite force. The two forces do not balance each other completely. The power balance is realised via the hydrodynamic lubrication on the slipper land. In addition, the flow rate changes somewhat with the runout on the slipper(r_{ro}) and the swash plate rotation rate (n). This, however, affects the slipper pocket pressure and the PD on the slipper. In the MGGP and ANN models, the variable input data were considered to predict the PD. Output data were taken for the pressure values measured on points 1, 2, and 3 of the slippers, depending on the angle (θ) value of the experimental setup. Thus,

$$P = f\left(P_s, P_r, Q, n, r_{ro}, \theta\right) \tag{12}$$

From the experiments, the following parameters were found to be most favourable: population size = 500, generation number = 400, tournament size = 15, Pareto tournament probability = 0.5, elite fraction = 0.08, $D_{max} = 6$, and $G_{max} = 6$. Hence, the equation yielding the most favourable PD was in

$$\begin{aligned} P = {} & 0.0588 + 0.00462\left(n + \left|r_{ro} - \theta + \tanh\left(n^2 r_{ro}\right)\right|\right. \\ & + \left|P_r\right| + \frac{\left(0.5P_s\right)}{\theta} \\ & \left. - \frac{\left(6.66e14\theta\right)}{\left(7.21e16\left(P_r - \theta\right) + 1.44e17\left|\theta\right|\right)}\right) + 0.0352\theta^2 \\ & + 0.127\left(P_s - \theta\right) \\ & + \frac{\left(4.58e15\tanh\left(n - \theta\right)\right)}{\left(7.21e16n + 3.6e16\left(Q_r^{1/2} - \theta^2\right)\right)} \\ & + \frac{\left(2.65e - 23\left(7.65e15\left(\theta - \exp n\right)\right)\right)}{\left(\theta + \left|P_r\right| + n/\theta^2 + P_s^3 - 9.29\right)^3} + 2.68e \\ & - 4\left(\tanh\left(P_s - \theta\right)\right. \\ & \left. - \left|n + \theta + \tanh\left(\theta\right) + \frac{\exp\left(P_s\right)}{\left|P_r\right|} + \frac{n}{\theta}\right| - n\theta^2 + Q_r^{1/2}\right. \\ & \left. - n^2 P_s r_{ro}\left(P_s - \theta\right)\right) \\ & - \frac{\left(1.08e - 19\left(9.91e14\left(n + \theta^6\right) + 1.98e15\theta\right)\right)}{\left|\theta + 2\left|P_r\right| + \left|\theta\right| + \exp P_s/n\right|} \end{aligned} \tag{13}$$

Table 4: Assessment of MO for the PD MLMs.

Models	Training Data	Test Data
P_{ANN}	0.7436	0.7990
P_{MGGP}	1.0219	1.0420

Table 5: Relative error (%) statistical performance for PD of MLMs.

Models	P_{MGGP}	P_{ANN}
Mean	1.0344	0.7933
LCI 95%	0.9611	0.7272
UCI 95%	1.1077	0.8593
Tr mean 5%	0.8760	0.6532
SD	1.1979	1.0792
Median	0.7387	0.5563
Min	0.0023	0.0014
Max	11.3905	13.9012

In the ANN model, however, two layers were used. The neuron numbers in the hidden layers (1-20) and the activation functions in (3)–(5) were tried, in all combinations. The model with the lowest MSE (2.6558e-05) had 16 and 13 neurons in the first and second hidden layers, respectively, and incorporated the tansig activation function.

Figure 7 shows the compatibility of the results for the training, validation, and test data given by the MGGP and ANN models with the experiment results for the PD on the slipper. It is apparent that both methods could learn very well during the training and validation stages (Figures 7(a) and 7(b)), with a very low error ratio. During the test stage, however, the ANN model could somewhat better predict the nonlinear relationship between the input and output variables, with a high R^2 value exceeding 0.99. The abundance of data enabled both models to achieve higher-accuracy predictions [13]. The MO values for both models were calculated on the training and test data, as detailed in Table 4.

The mean statistical performance, lower confidence interval (LCI) of the mean at 95%, upper confidence interval (UCI) of the mean at 95%, trimmed mean (Tr mean) 5%, standard deviation (SD), median, minimum (Min), and maximum (Max) are summarised in Table 5.

The low MO values on the test data, the LCI, and the low values of the other statistical data suggest that the ANN model exhibited somewhat superior performance to the MGGP model. Table 6 presents a comparison of the developed MLMs with AE derived from classical Reynolds equations. AE that comply with the measurement principles of the experiment setup were used.

AE-1 was derived by assuming that the pressure does not change throughout the angle and vibration, without considering flow rate. However, a hydrodynamic oil wedge is formed by the rotation of the swash plate. Therefore, small differences are observed in pressure measurement points. In Table 6, it is clear that the MLMs produced superior results to AE-1.

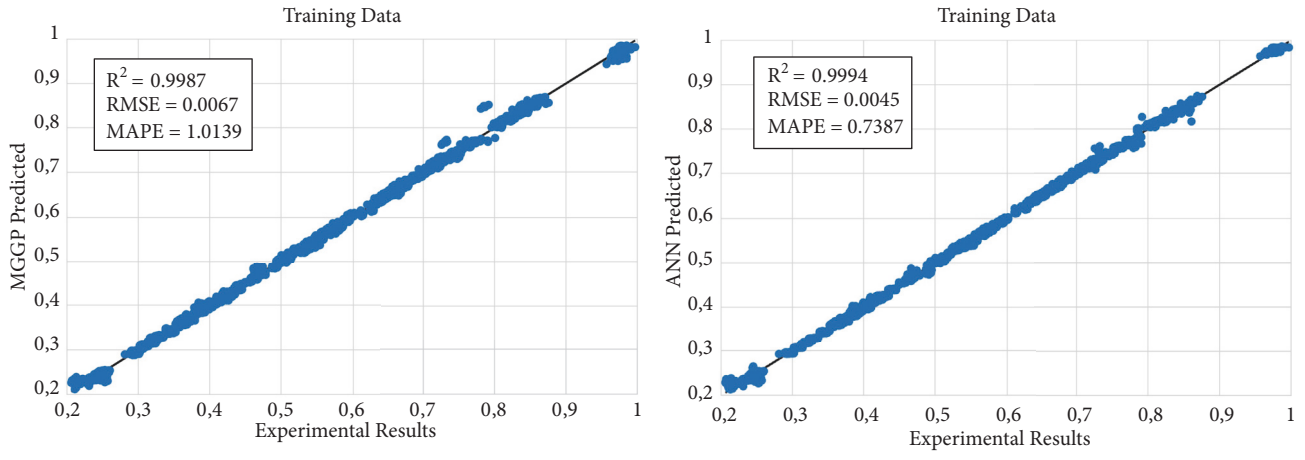

(a)

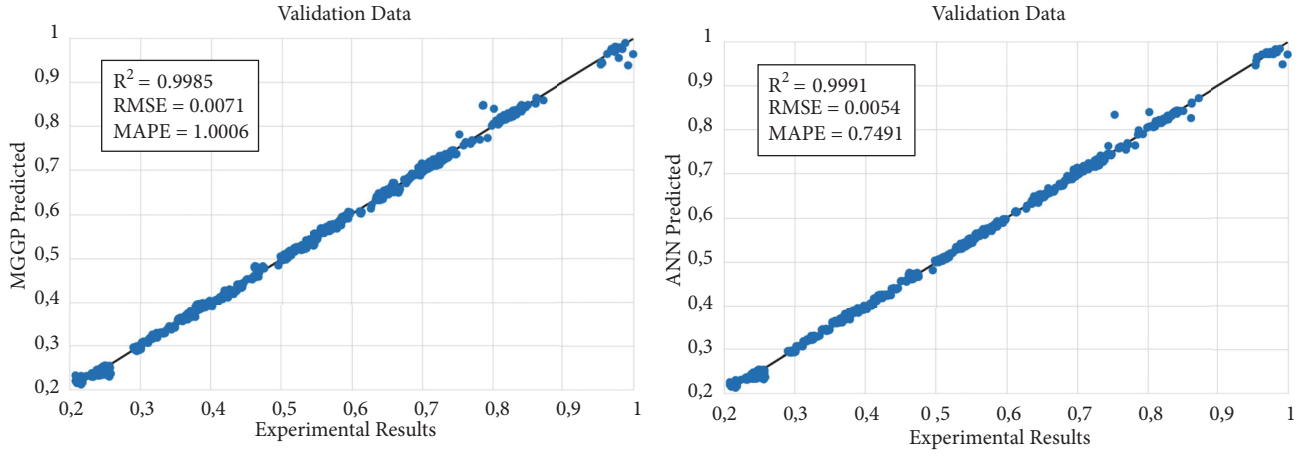

(b)

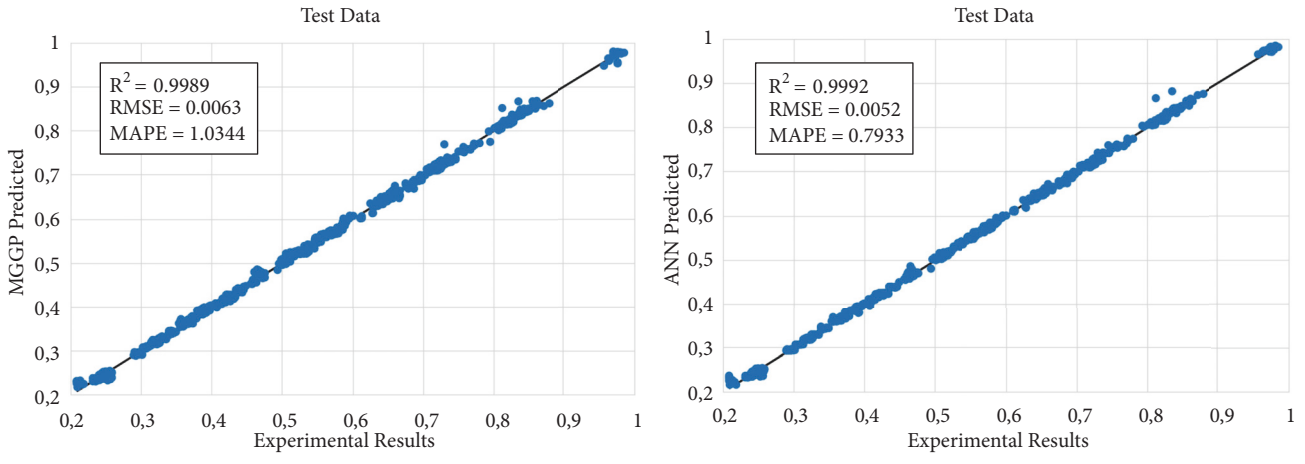

(c)

Figure 7: (a) Training data, (b) validation data, and (c) compatibility to test data, of the models developed with MLMs for PD.

Table 6: Comparison of AE with MLMs for PD.

Models	Performance			
	R^2	*RMSE*	*MAPE*	*MO*
AE-1 [2]	0.6650	0.1089	16.0833	24.3492
MGGP	0.9989	0.0063	1.0344	1.0420
ANN	0.9992	0.0052	0.7933	0.7990

Table 7: Evaluation of the MO error of MLMs for leakage.

Models	Training Data	Test Data
Q_{ANN}	0.0002	0.0003
Q_{MGGP}	0.0752	0.0689

Table 8: Relative error % statistical performance of MLMs for leakage.

Models	Q_{MGGP}	Q_{ANN}
Mean	0.068156	0.000276
LCI 95%	0.061743	0.000234
UCI 95%	0.074568	0.000319
Tr mean 5%	0.061236	0.000216
SD	0.0629866	0.0004211
Median	0.052302	0.000179
Min	0.0000	0.0000
Max	0.3704	0.0040

5.2. Leakage on the Slipper. The flow between a slipper with small clearance and the swash plate in an APP is generally considered to be laminar. This flow has an effect proportional to the amplitude of the runout on the flow and the thickness of the oil film [2]. For leakage, the mean of the runout measured on the slipper was computed (r_{av}). In addition, normalised logarithms of the output data were considered in order to determine the leakage quantity measured for the experiment setup, within (14). The leakage in this study is limited to the slipper/swash plate pair.

$$Q = f\left(P_s, P_r, n, r_{av}\right) \tag{14}$$

In the trials, a population size of 500, generation number of 400, tournament size of 15, Pareto tournament probability of 0.6, elite fraction of 0.1, D_{max} of 6, and G_{max} of 6 were found to be the best parameters. The equation yielding the best leakage result was as follows:

$$\begin{aligned} Q = {} & 0.696 + \frac{2.76e28\left(n + P_r\right)}{\left(2.31e31P_r^3 - 5.99e31\right)} - \frac{(4.34e-19)\left(7.83e15\left(n + \exp\left(P_s^{1/2}\right) + P_s^{1/2}\right)\right)}{\exp\left(\exp\left(P_s\right)^{1/2}\right)^{1/2}} + (4.52e-5)\exp\left(\exp\left(P_s\right)^{1/2}\right)^{1/4} \\ & + 0.0328\left(P_s - 7.76r_{av} - 1.0\tanh\left(P_s r_{av}\right)^{1/2}\right)^{1/2} \\ & + \frac{\left(5.81e15\left(n + n^2 + P_s^{1/2}\right) - 3.93e16\right)}{\left(2.95e20\left(n - \exp\left(P_s\right)\right) - (1.97e-5)\left(nabs\left(P_r^{1/2} - 1.0n + P_s^2\right) - n\left(n + P_s\right)\right)\right)} - 9.89\exp\left(-1.0P_r^2 - 2.3\right) \\ & \cdot \tanh\left(P_s r_{av}\right)^{1/2}\left(P_r + 2.0r_{av}\right) \end{aligned} \tag{15}$$

For the ANN model, the parameters in Section 4.1.1 were used, along with the tangent sigmoid function in the hidden layers and the pure linear activation function in the output layer; hence, the lowest MSE of 1.4605e-11 was obtained, with 19 and 14 neurons in the first and second hidden layers, respectively.

Figure 8 shows the compatibility of the training, validation, and test data for leakage obtained in experiment with the MGGP and ANN model results. For a flat slipper, the leakage change increases as the inlet pressure rises, but decreases by a certain degree as its rotation speed increases [2]. As apparent from Figure 8, this relationship can allow creation of highly predictive models using either of the developed MLMs. In this study, similar to existing ANN models designed to model the slipper flow rate [15], high predictive values were obtained. The ANN model was slightly more efficient than MGGP. The MO values for the leakage prediction of the MLMs were computed for the training and test data; the results are listed in Table 7. In addition, the statistical performance of the two MLMs for leakage is summarised in Table 8.

From the low statistical values, which were obtained because the leakage data were in a more definable range, it is apparent that the ANN model exhibited superior performance to the MGGP. Furthermore, a comparison of the results with AE is presented in Table 9.

AE-2 shows the flow on the orifice. Because the 0.9 mm diameter orifice is used, the inertia effects of the flow are effective [15]. AE-3 shows the flow between the slipper/swash plates. According to Table 9, although the AEs exhibited satisfactory performance as regards leakage, the MLMs displayed superior performance.

6. Conclusion

In this study, an alternative approach to modelling PD and leakage, which directly affect the friction and wear of the slipper of an APP, was presented; the proposed approach is based on MGGP and ANN MLMs. Data were obtained using a specially designed experiment setup. To assess the efficiency of the suggested models, data excluded from the analyses was employed as test data. Additionally, the results were compared with AEs reported in the literature, which were obtained with acceptances on the basis of the Reynolds equation. Compatible parameter sets were determined for both MLMs by taking parameters employed for similar

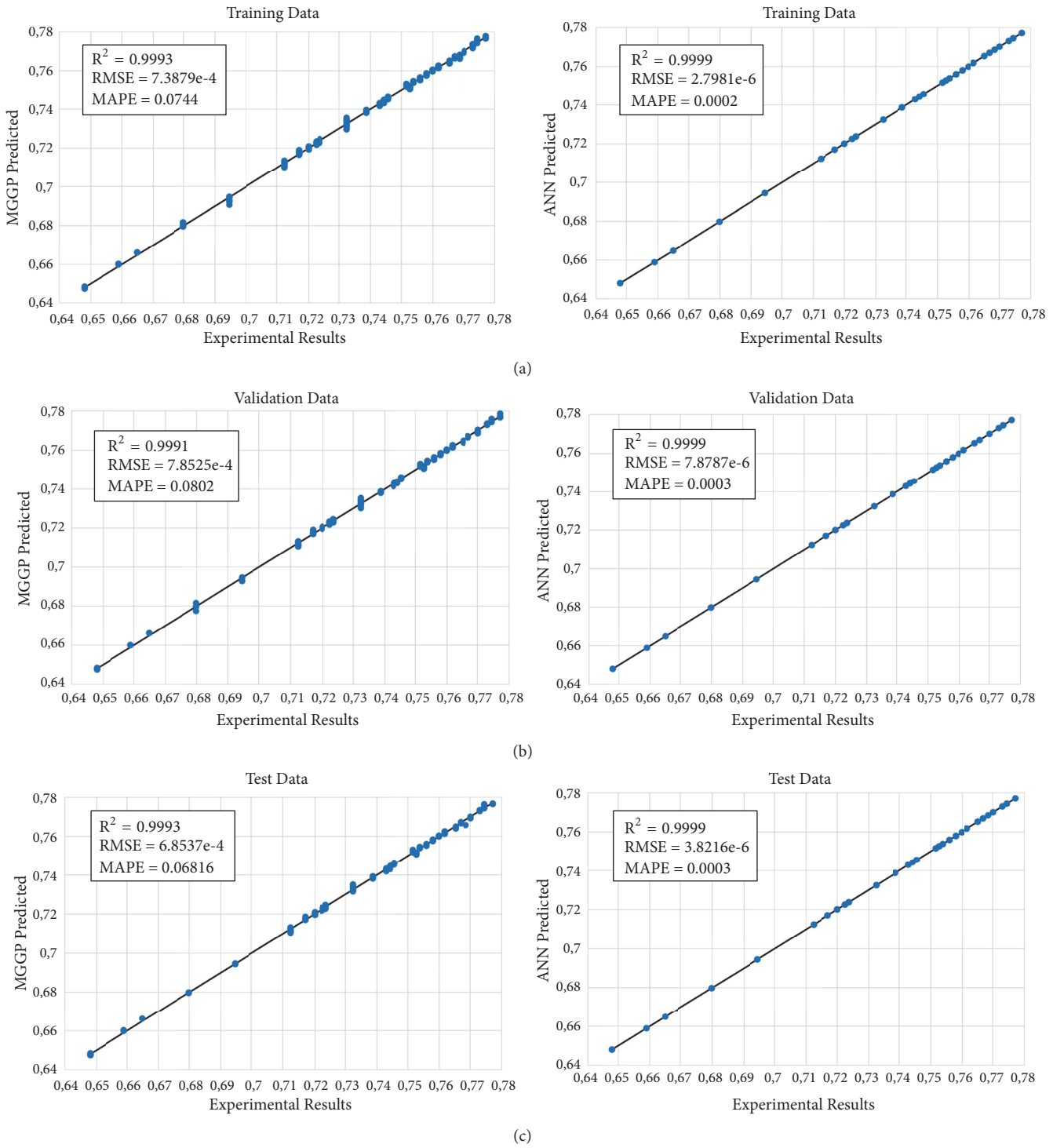

Figure 8: The compatibility of the models produced with MLMs to (a) training data, (b) validation data, and (c) test data.

problems in the literature as references and through the trial and error method.

The results revealed that both MLMs have high predictive performance as regards PD and leakage. The AEs, however, exhibited inferior performance to the MLMs, as they are based on certain assumptions, such as ignoring inertia and system noise. But it should be noted that analytical equations are more meaningful to define physical relationships mathematically. As for the ANN, although it exhibited superior performance to the MGGP, it could not produce a mathematical model. The proposed MLMs can be used as a preliminary design stage by engineers. The current study was restricted to the steady conditions and operational parameters of the slipper. In the future, through investigations focusing on

Table 9: Comparison of AEs with MLMs for leakage.

Model	Performance			
	R^2	*RMSE*	*MAPE*	*MO*
AE-2 [16]	0.8534	0.0099	0.8621	1.0218
AE-3 [2]	0.9932	0.0021	0.2629	0.2668
MGGP	0.9993	6.8537e-4	0.0681	0.0689
ANN	0.9999	3.8216e-6	0.0003	0.0003

the rotation operational conditions of the slippers, different slipper geometries, sudden load changes, the oil temperature effect, and the operational duration, a multipurpose model will be produced using strong optimisation algorithms considering all axial piston pumps.

Nomenclature

PD: Pressure distribution
APP: Axial piston pump
MGGP: Multigene genetic programming
ANN: Artificial neural network
MLMs: Machine learning methods
AEs: Analytic equations
GA: Genetic algorithm
GP: Genetic programming
MO: Multiobjective error
MAPE: Mean absolute percentage error
RE: Relative error
RMSE: Root mean square error
MSE: Mean squared error.

Data Availability

The data of the current study are available from the corresponding author upon acceptable request.

Conflicts of Interest

The authors declare that there are no conflicts of interest regarding the publication of this paper.

Acknowledgments

We would like to thank Editage [https://www.editage.com/] for editing and reviewing this manuscript's language. This work was supported by the Erciyes University Scientific Research Projects Coordination Unit, Project No. FDK-2016-6986.

References

[1] J. M. Bergada, J. M. Haynes, and J. Watton, "Leakage and groove pressure of an axial piston pump slipper with multiple lands," *Tribology Transactions*, vol. 51, no. 4, pp. 469–482, 2008.

[2] J. M. Bergada, J. Watton, J. M. Haynes, and D. L. Davies, "The hydrostatic/hydrodynamic behaviour of an axial piston pump slipper with multiple lands," *Meccanica*, vol. 45, no. 4, pp. 585–602, 2010.

[3] S. Kumar, J. M. Bergada, and J. Watton, "Axial piston pump grooved slipper analysis by CFD simulation of three-dimensional NVS equation in cylindrical coordinates," *Computers & Fluids*, vol. 38, no. 3, pp. 648–663, 2009.

[4] R. E. Johnson and N. D. Manring, "Translating circular thrust bearings," *Journal of Fluid Mechanics*, vol. 530, pp. 197–212, 2005.

[5] H.-S. Tang, Y.-B. Yin, Y. Zhang, and J. Li, "Parametric analysis of thermal effect on hydrostatic slipper bearing capacity of axial piston pump," *Journal of Central South University*, vol. 23, no. 2, pp. 333–343, 2016.

[6] H. Tang, Y. Yin, Y. Ren, J. Xiang, and J. Chen, "Impact of the thermal effect on the load-carrying capacity of a slipper pair for an aviation axial-piston pump," *Chinese Journal of Aeronautics*, vol. 31, no. 2, pp. 395–409, 2017.

[7] F. Canbulut, C. Sinanoğlu, and E. Koç, "Experimental analysis of frictional power loss of hydrostatic slipper bearings," *Industrial Lubrication and Tribology*, vol. 61, no. 3, pp. 123–131, 2009.

[8] F. Canbulut, "The experimental analyses of the effects of the geometric and working parameters on the circular hydrostatic thrust bearings," *JSME International Journal Series C Mechanical Systems, Machine Elements and Manufacturing*, vol. 48, no. 4, pp. 715–722, 2005.

[9] S. Lin and J. Hu, "Tribo-dynamic model of slipper bearings," *Applied Mathematical Modelling*, vol. 39, no. 2, pp. 548–558, 2015.

[10] Q. Chao, J. Zhang, B. Xu, and Q. Wang, "Discussion on the Reynolds equation for the slipper bearing modeling in axial piston pumps," *Tribology International*, vol. 118, pp. 140–147, 2018.

[11] J. Zhang, Q. Chao, Q. Wang, B. Xu, Y. Chen, and Y. Li, "Experimental investigations of the slipper spin in an axial piston pump," *Measurement*, vol. 102, pp. 112–120, 2017.

[12] H. Tang, Y. Ren, and J. Xiang, "A novel model for predicting thermoelastohydrodynamic lubrication characteristics of slipper pair in axial piston pump," *International Journal of Mechanical Sciences*, vol. 124, pp. 109–121, 2017.

[13] A. H. Gandomi and A. H. Alavi, "A new multi-gene genetic programming approach to nonlinear system modeling. Part I: materials and structural engineering problems," *Neural Computing and Applications*, vol. 21, no. 1, pp. 171–187, 2012.

[14] F. Canbulut, C. Sinanoğlu, and Ş. Yıldırım, "Analysis of effects of sizes of orifice and pockets on the rigidity of hydrostatic bearing using neural network predictor system," *KSME International Journal*, vol. 18, no. 3, pp. 432–442, 2004.

[15] F. Canbulut, C. Sinanoğlu, and Ş. Yildirim, "Neural network analysis of leakage oil quantity in the design of partially hydrostatic slipper bearings," *Industrial Lubrication and Tribology*, vol. 56, no. 4, pp. 231–243, 2004.

[16] F. Canbulut, Ş. Yıldırım, and C. Sinanoğlu, "Design of an artificial neural network for analysis of frictional power loss of

hydrostatic slipper bearings," *Tribology Letters*, vol. 17, no. 4, pp. 887–899, 2004.

[17] F. Canbulut, C. Sinanoğlu, Ş. Yildirim, and E. Koç, "Design of neural network model for analysing hydrostatic circular recessed bearings with axial piston pump slipper," *Industrial Lubrication and Tribology*, vol. 56, no. 5, pp. 288–299, 2004.

[18] H. Liu, Z. Peng, and C. Shen, "Film shape research of slipper bearing in axial piston pump based on Genetic Algorithms," *Advanced Materials Research*, vol. 301, pp. 1533–1538, 2011.

[19] F. Canbulut, C. Sinanoğlu, M. Erkilet, and Ö. Özmen, "Neural predictor to analyse the efficiency of positive displacement pumps," *Journal of the Balkan Tribological Association*, vol. 18, no. 4, pp. 530–539, 2012.

[20] J. R. Koza, "Genetic programming as a means for programming computers by natural selection," *Statistics and Computing*, vol. 4, no. 2, pp. 87–112, 1994.

[21] A. Garg, A. Garg, K. Tai, and S. Sreedeep, "An integrated SRM-multi-gene genetic programming approach for prediction of factor of safety of 3-D soil nailed slopes," *Engineering Applications of Artificial Intelligence*, vol. 30, pp. 30–40, 2014.

[22] J. Enríquez-Zárate, L. Trujillo, S. de Lara et al., "Automatic modeling of a gas turbine using genetic programming: an experimental study," *Applied Soft Computing*, vol. 50, pp. 212–222, 2017.

[23] A. H. Gandomi, A. H. Alavi, P. Arjmandi, A. Aghaeifar, and R. Seyednour, "Genetic programming and orthogonal least squares: a hybrid approach to modeling the compressive strength of CFRP-confined concrete cylinders," *Journal of Mechanics of Materials and Structures*, vol. 5, no. 5, pp. 735–753, 2010.

[24] A. H. Zaji and H. Bonakdari, "Application of artificial neural network and genetic programming models for estimating the longitudinal velocity field in open channel junctions," *Flow Measurement and Instrumentation*, vol. 41, pp. 81–89, 2015.

[25] M.-I. Kim and P. Zou, "Modeling of drilling forces based on twist drill point angles using multigene genetic programming," *Mathematical Problems in Engineering*, vol. 2016, Article ID 6749182, 9 pages, 2016.

[26] D. P. Searson, D. E. Leahy, and M. J. Willis, "GPTIPS: an open source genetic programming toolbox for multigene symbolic regression," in *Proceedings of the International Multiconference of Engineers and Computer Scientists*, vol. 1, pp. 77–80, 2010.

[27] D. P. Searson, GPTIPS: Genetic Programming & Symbolic Regression for MATLAB, User Guide, 2010.

[28] G. A. Morrison, D. P. Searson, and M. J. Willis, "Using genetic programming to evolve a team of data classifiers," *World Academy of Science, Engineering and Technology*, vol. 72, pp. 261–264, 2010.

[29] A. Garg, L. Rachmawati, and K. Tai, "Classification-driven model selection approach of genetic programming in modelling of turning process," *The International Journal of Advanced Manufacturing Technology*, vol. 69, no. 5-8, pp. 1137–1151, 2013.

[30] A. Garg, K. Tai, and M. M. Savalani, "State-of-the-art in empirical modelling of rapid prototyping processes," *Rapid Prototyping Journal*, vol. 20, no. 2, pp. 164–178, 2014.

[31] A. Garg, S. Sriram, and K. Tai, "Empirical analysis of model selection criteria for genetic programming in modeling of time series system," in *Proceedings of the Computational Intelligence for Financial Engineering & Economics (CIFEr)*, pp. 90–94, 2013.

[32] V. Vijayaraghavan, A. Garg, J. S. L. Lam, B. Panda, and S. S. Mahapatra, "Process characterisation of 3D-printed FDM components using improved evolutionary computational approach," *The International Journal of Advanced Manufacturing Technology*, vol. 78, no. 5-8, pp. 781–793, 2015.